Geoscientific
Model Development
Discussions

Open Access

Inherently mass-conservative version of the semi-Lagrangian Absolute Vorticity (SL-AV) atmospheric model dynamical core

V. V. Shashkin[1,2] **and M. A. Tolstykh**[1,2]

[1]Institute of Numerical Mathematics, Russian Academy of Sciences, 8, Gubkina st., 119333 Moscow, Russia
[2]Hydrometeorological centre of Russia, 11–13, Bol. Predtechenskiy lane, 123242 Moscow, Russia

Correspondence to: V. V. Shashkin (vvshashkin@gmail.com)

Discussion Paper | Discussion Paper | Discussion Paper | Discussion Paper |

GMDD

6, 4809–4832, 2013

Mass-conservative SL-AV

V. V. Shashkin and M. A. Tolstykh

Title Page

Abstract	Introduction
Conclusions	References
Tables	Figures

|◄ | ►|
| ◄ | ► |

Back | Close

Full Screen / Esc

Printer-friendly Version

Interactive Discussion

Abstract

The semi-Lagrangian Absolute Vorticity (SL-AV) atmospheric model is the global semi-Lagrangian hydrostatic model used for operational medium-range and seasonal forecasts at Hydrometeorological centre of Russia. The distinct feature of SL-AV dynamical core is the semi-implicit semi-Lagrangian vorticity-divergence formulation on the unstaggered grid. Semi-implicit semi-Lagrangian approach allows for long time steps while violates the global and local mass-conservation. In particular, the total mass in simulations with semi-Lagrangian models can drift significantly if no aposteriori mass-fixing algorithms are applied. However, the global mass-fixing algorithms degrade the local mass conservation.
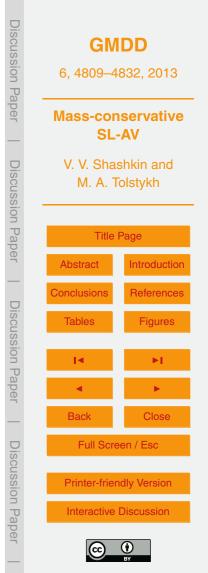
The inherently mass-conservative version of SL-AV model dynamical core presented in the article ensures global and local mass conservation without mass-fixing algorithms. The mass conservation is achieved with the introduction of the finite-volume semi-Lagrangian discretization for continuity equation based on the 3-D extension of the conservative cascade semi-Lagrangian transport scheme (CCS). The numerical experiments show that the presented new version of SL-AV dynamical core combines the accuracy and stability of the standard SL-AV dynamical core with the mass-conservation properties. The results of the mountain induced Rossby wave test and baroclinic instability test for mass-conservative dynamical core are found to be in agreement with the results available in literature.

1 Introduction

2 Motivation for the research

The modern atmospheric models used for long-range forecasting or climate change modeling should treat concentrations of the greenhouse gases and some other atmospheric constituents as prognostic variables. The constituents dynamics in the

absence of the chemical transformations is characterized by the local and global mass conservation. The both conservation properties should be maintained by the numerical method employed, since the global mass drift can introduce biases to the model feedback to the radiative forcing and the lack of the local conservation may
5   contaminate the physical sources and sinks of the constituents masses due to the chemical transformations.

Treatment of the atmospheric constituent concentrations as the prognostic variables is a difficulty for the semi-Lagrangian (SL) models which are well known to violate both local and global mass-conservation. In particular, the total mass of the atmosphere
10 and the mass of its constituents was found to drift significantly during the long-range integration of the SL models (see Bates et al., 1993, for example). The global mass correction approach (like Priestley , 1993) used in some SL models obviously degrades the local mass-conservation properties.

Despite the abovementioned mass conservation issues, the semi-implicit semi-
15 Lagrangian (SISL) treatment of the atmospheric equations is very suitable to be the core of the general circulation models because of its computational efficiency. Attempts are made to develop the advection schemes and the atmospheric equations discretizations that combine mass-conservation properties with the efficiency and robustness of the SL approach. Zerroukat and Allen (2012) presents the 3-D inherently
20 mass-conservative transport scheme on the sphere. CSLAM (Lauritzen et al., 2010) locally mass-conservative 2-D SL scheme on the cubed sphere provides the transport computations with the great multi-tracer efficiency. The approach for consistent coupling between the discrete tracer transport and continuity equations in the SISL shallow water model is implemented by Wong et al. (2013). Lauritzen et al. (2008)
25 develop the inherently mass-conservative limited area SL dynamical core for HIRLAM model using floating Lagrangian vertical levels.

This article presents the cell-integrated mass-conservative discretization of the continuity equation in the SISL framework for the SL-AV global atmospheric dynamical core. Unlike Lauritzen et al. (2008), fixed vertical levels are used. We consider

this research as a first step towards the hydrostatic SL dynamical core with mass-conservative and consistent tracer transport (as discussed in Wong et al., 2013), although the tracer transport problems are beyond the scope of the article.

2.1 Brief model overview

The SL-AV (semi-Lagrangian absolute vorticity) is the global semi-Lagrangian hydrostatic atmospheric model. The model includes the dynamical core developed in the Institute of Numerical Mathematics, Russian Academy of Sciences in cooperation with the Hydrometeorological centre of Russia and the subgrid scale physics package from ALADIN/LACE NWP model. The main feature of the SL-AV dynamical core is the finite-difference semi-implicit semi-Lagrangian formulation on the unstaggered grid with the horizontal divergence and the vertical component of the absolute vorticity as the prognostic variables. The horizontal grid is regular latitude-longitude with the options for the variable latitude resolution and the usage of the reduced lat–lon grid. In the vertical, sigma $\sigma = p/p_s$ (p is the pressure and p_s is the surface pressure) coordinate is used.
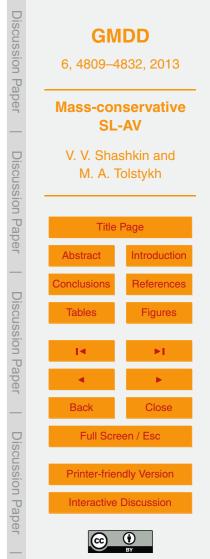
Medium-range and seasonal forecast versions of the SL-AV are operational at the Hydrometeorological centre of Russia. New versions of the model are being developed now. In particular, they are the non-hydrostatic version for the medium-range forecast and the hydrostatic mass-conservative version for long-range forecast and climate simulations.

2.2 Article structure

Section 3 presents the formulation of the inherently mass-conservative SISL dynamical core, beginning with the set of the atmospheric governing equations (dry, adiabatic) used (Sect. 3.1). The inherently mass-conservative dynamical core makes use of absolute vorticity, divergence and thermodynamical equations approximations along with the semi-implicit system formulation and many other discretizations from the

Title Page

Abstract | Introduction

Conclusions | References

Tables | Figures

|◄ | ►|

◄ | ►

Back | Close

Full Screen / Esc

Printer-friendly Version

Interactive Discussion

standard non-conservative SL-AV model dynamical core. Non-conservative dynamical core is overviewed in Sect. 3.2. Section 3.3 describes mass-conservative discretization of the continuity equation introduced to obtain mass-conservative dynamical core. Section 4 presents the results of numerical experiments.

3 Inherently mass-conservative SL dynamical core formulation

3.1 Governing equations

The governing equations for the SL-AV model dynamical core in absence of humidity are the adiabatic primitive equations written in the σ vertical coordinate as follows:

- the momentum equation in the vector form (Bates et al., 1993) with advected Coriolis term (Rochas , 1990):

$$\left(\frac{\mathrm{d}\boldsymbol{V}}{\mathrm{d}t} + 2\boldsymbol{\Omega} \times \frac{\mathrm{d}\boldsymbol{r}}{\mathrm{d}t}\right)_{\mathrm{H}} = -\nabla\Phi - RT\nabla\ln p_{\mathrm{s}}, \tag{1}$$

Since the prognostic variables are the horizontal divergence and the vertical component of the absolute vorticity, the momentum equations are used only to derive the absolute vorticity and divergence equations (see below).

- the heat and continuity equations with the orographic terms (Ritchie and Tanguay, 1996) to make spurious orographic resonance less severe:

$$\frac{\mathrm{d}T}{\mathrm{d}t} - \frac{RT}{c_p}\left(\frac{\dot{\sigma}}{\sigma} + \frac{\mathrm{d}\left(\ln p_{\mathrm{s}} + \frac{\Phi_{\mathrm{s}}}{R\bar{T}}\right)}{\mathrm{d}t}\right) = -\frac{1}{c_p}\boldsymbol{V}\cdot\nabla\Phi_{\mathrm{s}}, \tag{2}$$

$$\frac{\mathrm{d}\left(\ln p_{\mathrm{s}} + \frac{\Phi_{\mathrm{s}}}{R\bar{T}}\right)}{\mathrm{d}t} + D + \frac{\partial\dot{\sigma}}{\partial\sigma} = \frac{1}{R\bar{T}}\boldsymbol{V}\cdot\nabla\Phi_{\mathrm{s}}, \tag{3}$$

4813

- and the hydrostatic balance equation:

$$\frac{\partial \Phi}{\partial \ln \sigma} = -RT,$$ (4)

$V = (u, v)$ is the horizontal velocity vector, $\boldsymbol{\Omega}$ is Earth angular velocity vector, Ω is Earth angular velocity, r is the vector joining Earth center and the given point at the surface, $(..)_H$ is the horizontal projection of the vector, Φ is the geopotential, p_s is the surface pressure, ∇ is the horizontal gradient operator, T is the temperature, R is the ideal gas constant, c_p is the specific heat capacity at constant pressure, $\dot{\sigma}$ is the vertical velocity in the σ coordinate system, Φ_s is the surface geopotential, $\bar{T}$ is the constant reference temperature, $D = \mathrm{div}_2(u, v)$ is the horizontal divergence at the σ-plane, and a is the Earth radius.

The absolute vorticity equation is obtained analytically from the component form of the momentum equation (1):

$$\frac{d}{dt}(\zeta + f) = -(\zeta + f)D - J,$$

$$J = \frac{R}{a^2 \cos \varphi}\left(\frac{\partial T}{\partial \lambda}\frac{\partial \ln p_s}{\partial \varphi} - \frac{\partial T}{\partial \varphi}\frac{\partial \ln p_s}{\partial \lambda}\right) - \frac{1}{a \cos \varphi}\left(\frac{\partial \dot{\sigma}}{\partial \lambda}\frac{\partial v}{\partial \sigma} - \cos \varphi \frac{\partial \dot{\sigma}}{\partial \varphi}\frac{\partial u}{\partial \sigma}\right),$$ (5)

where ζ is the relative vorticity and $f = 2\Omega \sin \varphi$ is the Coriolis parameter, (λ, φ) are the longitude and the latitude respectively. The equation for the horizontal divergence D is obtained in the discrete form in Sect. 2.2.

The formulation of the mass-conservative dynamical core also requires the continuity equation to be rewritten in the integral form:

$$\frac{d}{dt}\int_{\delta V(t)} p_s dV = 0,$$ (6)

where $\delta V(t)$ is an arbitrary 3-D reference volume moving with the air.

Mass-conservative SL-AV

V. V. Shashkin and
M. A. Tolstykh

Title Page

Abstract | Introduction

Conclusions | References

Tables | Figures

|◀ | ▶|

◀ | ▶

Back | Close

Full Screen / Esc

Printer-friendly Version

Interactive Discussion

3.2 Basic (non-conservative) SL-AV dynamical core formulation

The SL-AV model uses the time stepping scheme based on SETTLS (Hortal , 2002) time approximation in combination with the semi-implicit approach and the pseudo-second order decentering (Temperton et al., 2001). The discrete time form of a generic equation

$$\frac{d\psi}{dt} + L\psi + N(\psi) = 0,$$

is as follows:

$$\frac{\psi^{n+1} - \psi_*^n}{\Delta t} + \frac{1}{2}\left(N(\psi)_*^{(n+1)_e} + N(\psi)^n\right) + \frac{1+\epsilon}{2}L\psi^{n+1} + \frac{1+\epsilon}{2}L\psi_*^n - \frac{\epsilon}{2}\left(L\psi_*^{(n+1)_e} + L\psi^n\right) = 0, \quad (7)$$

where ψ is an arbitrary variable, L and N are the linear and non-linear operators respectively, $\psi^{(n+1)_e} = 2\psi^n - \psi^{n-1}$, Δt is the time step, ϵ is the small decentering parameter, the notation ψ_* means the value of ψ calculated at the departure point of the upstream semi-Lagrangian trajectory. The ψ variable can be one of prognostic variables ζ, T or $\ln p_s$, the time-discrete forms of the corresponding equations are:

– absolute vorticity equation

$$(\zeta + f)^{n+1} - (\zeta + f)_*^n = -\frac{\Delta t}{2}\left[(1+\epsilon)\left((fD)^{n+1} + (fD)_*^n\right) - \epsilon\left((fD)_*^{(n+1)_e} + (fD)^n\right)\right.$$
$$\left. + \left\{\zeta D + J\right\}_*^{(n+1)_e} + \left\{\zeta D + J\right\}^n\right], \quad (8)$$

- thermodynamic equation linearized around the reference temperature $\bar{T}$

$$T^{n+1} - \kappa\bar{T}\left(\ln p_s + \frac{\Phi_s}{R\bar{T}} + \frac{(1+\epsilon)\Delta t}{2}\frac{\dot{\sigma}}{\sigma}\right)^{n+1} = T_*^n - \kappa\bar{T}\left(\ln p_s + \frac{\Phi_s}{R\bar{T}} - \frac{(1+\epsilon)\Delta t}{2}\frac{\dot{\sigma}}{\sigma}\right)_*^n$$

$$-\frac{\epsilon\Delta t}{2}\left(\left(\frac{\dot{\sigma}}{\sigma}\right)^n + \left(\frac{\dot{\sigma}}{\sigma}\right)_*^{(n+1)_e}\right) + \frac{1}{2}\left((N_T)^n + (N_T)_*^{(n+1)_e}\right)\Delta t, \tag{9}$$

- continuity equation (the notation $(.)_{*2}$ implies that horizontal 2-D interpolation is used to calculate departure point values)

$$\frac{\left(\ln p_s + \frac{\Phi_s}{R\bar{T}}\right)^{n+1} - \left(\ln p_s + \frac{\Phi_s}{R\bar{T}}\right)_{*2}^n}{\Delta t} = -\frac{1+\epsilon}{2}\left(D_3^{n+1} + D_{3*}^n\right) + \frac{\epsilon}{2}\left(D_3^n + D_{3*}^{(n+1)_e}\right)$$

$$+\frac{1}{2R\bar{T}}\left(\mathbf{V}^n\nabla\Phi_s + \mathbf{V}_*^{(n+1)_e}\nabla\Phi_{s*}\right), \tag{10}$$

$D_3 = D + \partial\dot{\sigma}/\partial\sigma$ is the 3-D divergence, $\kappa = \frac{R}{c_p} = \frac{2}{7}$, N_T stands for the non-linear terms of the thermodynamic equation.

The vertical part of D_3^{n+1} i.e. $\partial\dot{\sigma}^{n+1}/\partial\sigma$ is contained in the time-discrete p_s equation (10). It can be excluded from (10) while integrating it from the model top $\sigma = \sigma_{top}$ to the model bottom $\sigma = 1$ using the boundary conditions $\dot{\sigma}(1) = \dot{\sigma}\left(\sigma_{top}\right) = 0$ and treating $\ln p_s$ as pseudo-3D variable constant in the vertical:

$$(1 - \sigma_{top})\ln p_s^{n+1} = \int_{\sigma_{top}}^{1}\left\{-\frac{\Phi_s}{R\bar{T}} + \left(\ln p_s + \frac{\Phi_s}{R\bar{T}}\right)_{*2}^n - \frac{1+\epsilon}{2}\Delta t\left(D^{n+1} + D_{3*}^n\right) + \frac{\epsilon}{2}\left(D_3^n + D_{3*}^{(n+1)_e}\right)\right.$$

$$\left.+\frac{1}{2R\bar{T}}\left(\mathbf{V}^n\nabla\Phi_s + \mathbf{V}_*^{(n+1)_e}\nabla\Phi_{s*}\right)\right\}d\sigma. \tag{11}$$

Title Page

Abstract | Introduction

Conclusions | References

Tables | Figures

◄◄ | ►►

◄ | ►

Back | Close

Full Screen / Esc

Printer-friendly Version

Interactive Discussion

The similar technique is applied to derive the expression for $\dot{\sigma}^{n+1}$ used in the energy conversion term of the thermodynamic equation (9). The continuity equation (10) is integrated from the model top to σ. Equation (11) is used to eliminate p_s:

$$\dot{\sigma}^{n+1}(\sigma) = \frac{2}{(1+\epsilon)\Delta t}\left(\int_{\sigma_{\text{top}}}^{\sigma}\{.\}\mathrm{d}\sigma - \frac{\sigma - \sigma_{\text{top}}}{1 - \sigma_{\text{top}}}\int_{\sigma_{\text{top}}}^{1}\{.\}\mathrm{d}\sigma\right) \tag{12}$$

5   The terms in the curved brackets $\{.\}$ are equal to the sub-integral term in the curved brackets from Eq. (11).

The time-discrete equation for the horizontal divergence is obtained with the application of the horizontal divergence operator $\mathrm{div}_2(a_1, a_2) = \frac{1}{a\cos\varphi}\left(\frac{\partial a_1}{\partial\lambda} + \frac{\partial a_2 \cos\varphi}{\partial\varphi}\right)$ to the component form of the momentum equation (1) linearized around $\bar{T}$ and written

10 in the time-discrete form, similar to (7):

$$D^{n+1} = -\frac{1+\epsilon}{2}\Delta t\nabla^2\left(\Phi + R\bar{T}\ln p_s\right)^{n+1} + \mathrm{div}_2(A_u^n, A_v^n), \tag{13}$$

the vector (A_u^n, A_v^n) is the combination of known time-step n quantities from the right hand side of the time-discrete momentum equation.

Equations (8), (9), (11), (12), and (13) compose the system for the variables

15 $\left(\zeta^{n+1}, T^{n+1}, \ln p_s^{n+1}, \dot{\sigma}^{n+1}, D^{n+1}\right)$. The system is closed with the hydrostatic equation (4) rewritten for Φ^{n+1}

$$\Phi^{n+1}(\sigma) = \Phi_s + R\int_{1}^{\sigma}T^{n+1}(\sigma)\mathrm{d}\ln\sigma, \tag{14}$$

Given D^{n+1}, all other variables can be easily computed using Eqs. (8), (9), (11), and (12). Thus it is reasonable to isolate D^{n+1} in the single equation. As in Bates

et al. (1993), we derive the D^{n+1} equation in the vertical discrete form on the non-uniform vertical grid of NLEV levels. The vertical grid is defined by the NLEV + 1 half-levels $\sigma_{k+1/2}$, $k = 0 \ldots$ NLEV such that $\sigma_{1/2} = \sigma_{\text{top}}$ and $\sigma_{\text{NLEV}+1/2} = 1$, the vertical levels are $\sigma_k = \frac{1}{2}(\sigma_{k+1/2} + \sigma_{k-1/2})$, $k = 1 \ldots$ NLEV, the vertical grid spacing $\Delta\sigma_k = (\sigma_{k+1/2} - \sigma_{k-1/2})$. The vertical part of 3-D divergence is discretized as

$$\frac{\partial\dot{\sigma}}{\partial\sigma} = \frac{\dot{\sigma}_{k+1/2} - \dot{\sigma}_{k-1/2}}{\Delta\sigma_k}. \qquad (15)$$

The vertical integration terms of p_s (11) and hydrostatic (14) equations are substituted for their discrete analogues using the medium point and trapezoidal rules respectively.

The elimination of $(T^{n+1}, \ln p_s^{n+1}, \Phi^{n+1})$ in divergence equation (13) using Eqs. (9), (11), (12), and (14) leads to the equation for D^{n+1}

$$D^{n+1} - \left(\frac{1+\epsilon}{2}\Delta t\right)^2 \nabla^2 \mathbf{M} D^{n+1} = H^n, \qquad (16)$$

where D^{n+1} is the vector of dimension NLEV with components D_k^{n+1}, $k = 1 \ldots$ NLEV representing the horizontal divergence at level σ_k as a function of (λ, φ). (Note that our considerations are still analytical in horizontal.) The vector H^n is a combination of known time-level n values. The matrix $\mathbf{M}$ of size NLEV × NLEV results from approximation of the integrals in Eqs. (11) and (14), the notation $\nabla^2 \mathbf{M} D^{n+1}$ means that horizontal ∇^2 operator is applied to each component of vector $\mathbf{M}D^{n+1}$.

To obtain the D^{n+1}, the problem (16) is reduced to NLEV horizontal Helmholtz equations using the eigenvalue transformation $\mathbf{M} = \mathbf{P}\Lambda\mathbf{P}^{\mathsf{T}}$ (see Bates et al., 1993, for details). The 2-D Helmholtz equations are solved on the regular latitude–longitude grid using the algorithm from Tolstykh (2002).

To summarize the description above, the structure of computations at the $n + 1$-th time step in the dynamical core is as follows:

1. The coordinates of the upstream trajectories departure points are computed using (u^n, v^n), (u^{n-1}, v^{n-1}) via the algorithm from Rochas (1990).

2. All departure point quantities i.e. the terms $(\ldots)_*^n$ of Eqs. (8), (10), (9), and (13) are calculated using interpolation.

3. The Helmholtz problem (16) is solved and divergence D^{n+1} is obtained.

4. The updates ζ^{n+1}, T^{n+1}, $\ln p_s^{n+1}$ are obtained from Eqs. (8), (9), and (11) using the departure point quantities and D^{n+1}.

5. The horizontal wind at $n+1$-th time step (u^{n+1}, v^{n+1}) is reconstructed from ζ^{n+1} and D^{n+1} using the solver described in Tolstykh and Shashkin (2012).

3.3 Mass-conservative SL discretization of the continuity equation

The mass of the air contained in the elementary volume $dV = a^2 \cos\varphi d\lambda d\varphi d\sigma$ in the hydrostatic atmosphere is $m = p_s(\lambda, \varphi)dV$. The total mass of the atmosphere is $M = \int p_s dV = (1 - \sigma_{top}) \int p_s dS$, where the first integral is assumed over the all atmosphere and the second integral is over the sphere.

To get the semi-implicit mass-conservative discrete equation for p_s, the integral form of the continuity equation (6) is linearized around $p_{ref}(\lambda, \varphi)$:

$$\frac{d}{dt} \int_{\delta V(t)} p_s' dV = - \int_{\delta V(t)} \left[\nabla (p_{ref} \boldsymbol{V}) + p_{ref} \frac{\partial \dot\sigma}{\partial \sigma} \right] dV \qquad (17)$$

$p_s' = p_s - p_{ref}$. In the right hand side of this equation, we have used the Eulerian treatment of the $\frac{d}{dt}\int$ and the fact that $\frac{\partial p_{ref}}{\partial t} = 0$ and $\frac{\partial p_{ref}}{\partial \sigma} = 0$. Following the strategy of the SL methods, the arrival cell $\delta V \left(t^{n+1} \right)$ supposed to coincide with some grid cell ΔV and the departure cell $\delta V(t^n) = \Delta V_*$ is then determined with the SL trajectory searching algorithm. Given the arrival and departure cells, Eq. (17) is discretized in time using the

Title Page

Abstract | Introduction

Conclusions | References

Tables | Figures

|◄ | ►|

◄ | ►

Back | Close

Full Screen / Esc

Printer-friendly Version

Interactive Discussion

same approach (7) as for the non-conservative continuity equation:

$$\frac{p_s'^{n+1} \Delta V - \int_{\Delta V_*} p_s'^n \, \mathrm{d}V}{\Delta t} =$$

$$-\frac{1+\epsilon}{2}\left(\left[\nabla \left(p_{\mathrm{ref}} \boldsymbol{V}^{n+1} \right) + p_{\mathrm{ref}} \frac{\partial \dot{\sigma}^{n+1}}{\partial \sigma} \right] \Delta V + \int_{\Delta V_*} \left[\nabla \left(p_{\mathrm{ref}} \boldsymbol{V}^{n} \right) + p_{\mathrm{ref}} \frac{\partial \dot{\sigma}^{n}}{\partial \sigma} \right] \mathrm{d}V \right)$$

$$+\frac{\epsilon}{2}\left(\left[\nabla \left(p_{\mathrm{ref}} \boldsymbol{V}^{n} \right) + p_{\mathrm{ref}} \frac{\partial \dot{\sigma}^{n}}{\partial \sigma} \right] \Delta V + \int_{\Delta V_*} \left[\nabla \left(p_{\mathrm{ref}} \boldsymbol{V}^{(n+1)_e} \right) + p_{\mathrm{ref}} \frac{\partial \dot{\sigma}^{(n+1)_e}}{\partial \sigma} \right] \mathrm{d}V \right) \quad (18)$$

The arrival cell integral of a function is treated here as the cell averaged value of the function multiplied by the arrival cell volume.

The mass-conservation properties of the continuity equation approximation (18) depend on the scheme used for the computation of the departure volume integrals and the approximation of $\nabla(p_{\mathrm{ref}} \boldsymbol{V})$ terms. As for the departure volume computations, we use 3-D extension of the conservative cascade scheme (CCS) by Nair et al. (2002). The CCS 3-D implies the approximation of the departure volume geometry by the polyhedron with the sides parallel to the coordinate planes $O\lambda\varphi$, $O\lambda\sigma$, $O\varphi\sigma$. Following the ideology of the cascade approach, the form of the polyhedron in CCS 3-D is chosen in a way to allow the splitting of the 3-D integration into the three consecutive 1-D integrations. Piecewise parabolic subgrid reconstruction (Colella and Woodward, 1984) without limiters and filters is used for the 1-D integral approximation.

The $\nabla(p_{\mathrm{ref}} \boldsymbol{V}) = \mathrm{div}_2(p_{\mathrm{ref}} u, p_{\mathrm{ref}} v)$-type terms are calculated with the 2-D divergence calculation algorithm from the mass conservative shallow water model Tolstykh and Shashkin (2012). The algorithm used guarantees $\int \nabla(p_{\mathrm{ref}} \boldsymbol{V}) \, \mathrm{d}S = 0$ (the integral is over the sphere) and thus in combination with CCS 3D ensures the mass-conservation of the continuity equation approximation (18) (see Tolstykh and Shashkin, 2012, for the detailed discussion).

Full Screen / Esc

Similarly to the non-conservative p_s equation (10), the mass-conservative one (18) contains the $(\partial \dot{\sigma}/\partial \sigma)^{n+1}$ term. As in the non-conservative case, Eq. (18) is integrated from the model top to the model bottom using the boundary conditions $\dot{\sigma}(1) = \dot{\sigma}(\sigma_{\text{top}}) = 0$ to eliminate the vertical velocity $\dot{\sigma}$. The vertical integration in the case of Eq. (18) is equal to sum over the vertical column of the arrival cells V_k, $k = 1 \ldots \text{NLEV}$ spreading from the model top to the model bottom. The resulting mass conservative p_s equation can be written as

$$
(1 - \sigma_{\text{top}}) p_s'^{n+1} \Delta S = \sum_{k=1}^{N} \left\{ \int_{\Delta V_{k*}} p_s'^{n} \mathrm{d}V - \frac{1+\epsilon}{2} \Delta t \left(\nabla \left(p_{\text{ref}} \boldsymbol{V}^{n+1} \right)_k \Delta V_k \right. \right.
$$

$$
+ \int_{\Delta V_{k*}} \left[\nabla \left(p_{\text{ref}} \boldsymbol{V}^n \right) + p_{\text{ref}} \frac{\partial \dot{\sigma}}{\partial \sigma}^n \right] \mathrm{d}V \right) + \frac{\epsilon}{2} \Delta t \left(\left[\nabla \left(p_{\text{ref}} \boldsymbol{V}^n \right)_k + p_{\text{ref}} \frac{\partial \dot{\sigma}}{\partial \sigma}^n \right] \Delta V_k
$$

$$
+ \int_{\Delta V_{k*}} \left[\nabla \left(p_{\text{ref}} \boldsymbol{V}^{(n+1)_e} \right) + p_{\text{ref}} \frac{\partial \dot{\sigma}}{\partial \sigma}^{(n+1)_e} \right] \mathrm{d}V \left. \left. \right) \right\} , \tag{19}
$$

where ΔS is the square of the base of the vertical column, ΔV_{k*} is the departure cell corresponding to the arrival cell ΔV_k, $\nabla \left(p_{\text{ref}} \boldsymbol{V} \right)_k$ refers to the value of $\nabla \left(p_{\text{ref}} \boldsymbol{V} \right)$ averaged over ΔV_k.

Equations (18) and (19) are used to derive the expression for $\dot{\sigma}^{n+1}$ to be used in the energy conversion term of the thermodynamic equation (9) consistent with the mass-conservative continuity equation approximation. Equation (18) is summed over the vertical column of cells V_k, $k = 1 \ldots K$, $K = 1 \ldots \text{NLEV} - 1$ and Eq. (19) is used to

eliminate p_s^{n+1}. The resulting equation for $\dot{\sigma}_{K+1/2}$ is

$$\sigma_{K+1/2}^{n+1} = \frac{2}{(1+\epsilon)\,p_{\text{ref}}\Delta t \Delta S} \left[\sum_{k=1}^{k=K} \{\ldots\} - \frac{\sigma_{K+1/2} - \sigma_{\text{top}}}{1 - \sigma_{\text{top}}} \sum_{k=1}^{k=N} \{\ldots\} \right], \qquad (20)$$

the terms in the curved brackets $\{\ldots\}$ are equal to the term in the curved brackets in Eq. (19).

The computational procedure of the $n+1$-th time step of the presented mass-conservative dynamical core is as follows

1. The coordinates of the departure points of the upstream trajectories are computed.

2. All departure point quantities, i.e. the terms $(\ldots)_*^n$ of Eqs. (8), (9), (10), and (13), and also the departure volume integrals from Eq. (19) are calculated.

3. The Helmholtz problem (16) is solved and divergence D^{n+1} is obtained. Note that non-conservative continuity equation (10) is still implicitly used in the Helmholtz equation system (16).

4. The ζ^{n+1} is calculated using Eq. (8).

5. The horizontal wind $\boldsymbol{V}^{n+1}$ is reconstructed from known D^{n+1} and ζ^{n+1}.

6. Given the horizontal wind, the term $\nabla\left(p_{\text{ref}}\boldsymbol{V}^{n+1}\right)$ is calculated and used to compute p_s^{n+1} and $\dot{\sigma}^{n+1}$ vertical velocity via Eqs. (19) and (20)

7. Given $\dot{\sigma}^{n+1}$, Eq. (9) is used to calculate T^{n+1}.

4 Numerical experiments

We test the presented mass-conservative version of the SL-AV model dynamical core (further denoted as SLAV-MC) with the mountain induced Rossby wave and the Jablonowski and Williamson (2006) baroclinic instability test cases. The tests are carried out using four regular grids with 400×250, 640×400, 800×500 and 1200×750 grid points in longitude and latitude, the corresponding horizontal grid spacings are $0.9° \times 0.72°$, $0.5625° \times 0.45°$, $0.45° \times 0.36°$, $0.3° \times 0.24°$ in longitude and latitude respectively. In the vertical, we use the set of 28 equally spaced levels with $\sigma_{\text{top}} = 10^{-3}$.

The implicit ∇^4 horizontal diffusion is applied for ζ, D and T in all tests. The resolution independent diffusion coefficients from the operational medium-range forecast model version are used: $K_\zeta = 1.27 \times 10^{15}\,\text{m}^4\,\text{s}^{-1}$, $K_D = 1.91 \times 10^{15}\,\text{m}^4\,\text{s}^{-1}$, $K_T = 1.91 \times 10^{15}\,\text{m}^4\,\text{s}^{-1}$. Also, the decentering parameter ϵ is set to 5×10^{-2} as in the operational version.

4.1 Mountain-induced Rossby wave

This 3-D analogue of the shallow water test case No. 5 from Williamson et al. (1992) is carried out to check the performance of the mass-conservative dynamical core in the presence of the orography. The test setup presented in Jablonowski et al. (2008) is used. The initial conditions present the hydrostatically balanced smooth zonal flow which is the stationary analytic solution to the primitive equations in the absence of the orography. Given the non-zero orography, the zonal flow breaks up and a Rossby wave train begins its evolution.

The SLAV-MC setup for the test uses the reference surface pressure $p_{\text{ref}} = p_0 \exp\left(-\Phi_S/RT_0\right)$ with $p_0 = 930\,\text{hPa}$ and $T_0 = 288\,\text{K}$ (equal to the initial isothermal state of the atmosphere). This choice of p_{ref} produces the Ritchie and Tanguay (1996) – like orographic correction terms in the mass-conservative continuity equation (17) that improved the SLAV-MC accuracy near the mountain. The reference temperature $\bar{T}$

Full Screen / Esc

Printer-friendly Version

Interactive Discussion

is set to 320 K. The time step for the 400 × 250 grid simulations is 3600 s. which gives the initial zonal CFL number $C \approx 0.72$. In higher resolution simulations, the time step is chosen to keep the CFL number the same.

Figure 1 presents the day 15 and day 25 geopotential height and temperature fields at 700 hPa from SLAV-MC simulations on the 400 × 250 and 1200 × 750 grids. The pictures in Fig. 1 from the 400 × 250 grid (the coarsest one in the study) and 1200 × 750 grid (the finest one) results looks practically identical, so one can conclude that SLAV-MC simulations for the used grids are converged. Using finer grid allows to catch finer features in the temperature field near the mountain. Also, we found that SLAV-MC results agree well with the example results provided in the Jablonowski et al. (2008) and with the standard (non mass-conservative) SLAV dynamical core results.

The SLAV-MC dynamical core conserves the global mass up to machine precision whereas the standard SLAV dynamical core with mass-fixer turned off produces the monotonic global mass decrease that amounts 0.02 % of the total atmosphere mass during the month integration of the test case initial conditions on the 640 × 400 grid. Such mass trend cannot be considered as negligible for integration periods longer than year.

4.2 Baroclinic instability test

The test case as described in Jablonowski and Williamson (2006) consists of two parts. The first part tests the ability of the dynamical core to maintain the steady-state initial conditions with two mid-latitude jets. The second part of the test consists of the same steady-state initial conditions with overlaid zonal wind speed perturbation starting the evolution of the baroclinic wave.

The time step for 400 × 250 grid simulations is 2700 s yielding the initial maximum zonal CFL number $C \approx 1.3$. In higher resolution simulations, the time step is chosen to keep the CFL number the same. The CFL number used is at least twice higher than one used by Jablonowski and Williamson (2006) in simulations with SL dynamical

core of the CAM3 model. The reference state used in the experiment is the constant $p_{\text{ref}} = 900\,\text{hPa}$ and $\bar{T} = 320\,\text{K}$ reference temperature.

In the first part (stationary case) of the test, the model deviation from the initial state (which is the analytic solution) is dominated by the numerical vertical integration error in the hydrostatic balance equation (14). This gives the root mean square l_2 error (as defined in Jablonowski and Williamson, 2006) in p_s field of about 0.2 hPa after 30 days integration. The error is reduced twice when increasing the number of vertical levels up to 50. The initial state is also affected by the Helmholtz solver boundary conditions near the poles which are only 2nd order accurate in the latitudinal direction. This produces the p_s decrease of about of 3 hPa around the poles in the simulations with the 400×250 regular grid. The p_s field remains symmetric under all test conditions.

In the second part of the test case (the steady state initial conditions with overlaid perturbation), we find that the SLAV-MC simulation results agree well with the reference solutions from Jablonowski and Williamson (2006) and with the results from the standard (non mass-conservative) SL-AV dynamical core. Also, it is found that the day 1 till day 9 p_s and T field pictures from the SLAV-MC runs at different resolutions are practically indistinguishable. For example, the only difference that can be directly observed between the day 9 snapshots of SLAV-MC solutions on 400×250 and 1200×750 grids (upper and middle row of Fig. 2 correspondingly) is the slightly deeper eastern cyclonic feature in the higher resolution run. Figure 2 also presents the snapshot from standard SLAV solution on 1200×750 grid (lower row) which is very similar to the SLAV-MC snapshots.

The quantitative assessment of the similarity and difference between numerical solutions is available via the l_1, l_2, l_∞ surface pressure difference norms defined in Jablonowski and Williamson (2006). The upper row in Fig. 3 presents the difference between the SLAV-MC solutions at various resolutions and the reference solution from the T340 spectral SL dynamical core of the CAM3 atmospheric model. The lower row of the figure shows the difference norms between the lower resolution SLAV-MC solutions and the the highest resolution (1200×750 lon–lat grid) SLAV-MC solution.

The gray shading on Fig. 3 denotes the uncertainty of the numerical solution obtained in Jablonowski and Williamson (2006) by comparing different reference solutions.

The difference norms shown on the upper row of Fig. 3 are all below the uncertainty limit. That confirms the convergence of SLAV-MC simulations to the reference solution. Also, one can see that the lower resolution SLAV-MC solutions converge to the highest resolution SLAV-MC solution (at 1200 × 750 grid) since the corresponding difference norms (lower panel of Fig. 3) fall below the uncertainty too. Finally, the difference norms between standard SLAV and SLAV-MC solutions of equal resolution are well below the uncertainty limit (not shown) that proves the similar behaviour of the two versions of the dynamical core.
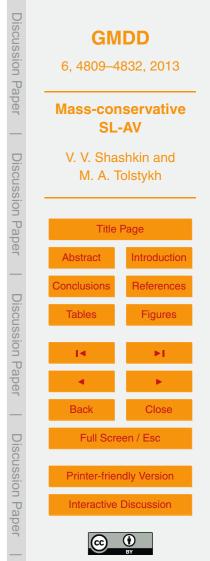
As in the mountain induced Rossby wave test case, the standard non-conservative SL-AV solution is characterized by the monotonic loss of the total mass. The value of mass loss (0.02 % of the total atmosphere mass on the 640 × 400 grid) is again too small to influence the test case numerical solution, but can contaminate the solution in longer term integrations.

5 Conclusions

Semi-implicit time integration scheme in conjunction with the semi-Lagrangian treatment of advection allows to run atmospheric simulations with time steps larger than time steps limited by CFL stability condition and thus to build computationally efficient models. Indeed, it was shown that the semi-Lagrangian advection can be implemented efficiently on massively parallel computer systems using up to $O(10^4)$ processors (White and Dongarra, 2011). Recently, it was found that the elliptic solver necessary to implement the semi-implicit scheme also can use such systems efficiently (see Müller and Sheichl, 2013). However, the application of SISL methods in modern atmospheric models used for climate simulations is limited by the absence of inherent mass-conservation requiring a global mass-fixer.

We presented a version of SISL dynamical core for the SL-AV global model which is inherently mass-conservative without use of mass correctors. The mass conservation is achieved by the introduction of the cell integrated semi-Lagrangian discretization for the continuity equation. This discretization is based on the 3-D extension of the Conservative Cascade SL transport Scheme (CCS) by Nair et al. (2002). Except for the new discretization of the continuity equation, approximation of the primitive equations and the semi-implicit equation system formulation in the mass-conservative version are the same as in the standard version, so only minimal changes to the dynamical core are introduced.

The numerical experiments showed that the inherently mass-conservative version of SL-AV dynamical core (SLAV-MC) is as accurate and stable with long time steps as the standard nonconservative version of this dynamical core. The results of SLAV-MC for the baroclinic instability test (Jablonowski and Williamson, 2006) and mountain induced Rossby-wave test (from Jablonowski et al., 2008) are found to be in agreement with the results available in literature. In the baroclinic instability test case, the difference norms between SLAV-MC solutions in various resolution and the reference T340 SL solution are below the solution uncertainty calculated in Jablonowski and Williamson (2006). The behavior of two versions of the dynamical core in the numerical experiments is very similar, except that the standard version (with mass-corrector turned off) produces the monotonic loss of global mass which can be crucial in the longer period simulations. SLAV-MC conserves the global mass up to machine precision.

The presented approach combines efficiently the advantages of the SISL method with the inherent mass conservation. Thus we believe that our research can be the base for building SISL dynamical core of an atmospheric general circulation model suitable for long range forecasting and climate simulations. In particular, we plan to implement the reduced lat–lon grid in our dynamical core, as we did for the shallow water model (Tolstykh and Shashkin, 2012). Also, consistent transport formulation similar to Wong et al. (2013) is considered.

Title Page

Abstract | Introduction

Conclusions | References

Tables | Figures

|◀ | ▶|

◀ | ▶

Back | Close

Full Screen / Esc

Printer-friendly Version

Interactive Discussion

References

Bates, J. R., Moorthi, S., and Higgins, R. W.: A global multilevel atmospheric model using a vector semi-Lagrahgian finite-difference scheme, Mon. Weather Rev., 121, 244–263, doi:10.1175/1520-0493(1993)121<0244:AGMAMU>2.0.CO;2, 1993. 4811, 4813, 4817, 4818

Colella, P. and Woodward, P. R.: The Piecewise Parabolic Method (PPM) for Gas-Dynamical Simulations, J. Comput. Phys., 54, 174–201, 1984. 4820

Hortal, M.: The development and testing of a new two-time-level semi-Lagrangian scheme (SETTLS) in the ECMWF forecast model, Q. J. Roy. Meteor. Soc., 128, 1671–1688, doi:10.1002/qj.200212858314, 2002. 4815

Jablonowski, C. and Williamson, D. L.: A baroclinic instability test case for atmospheric model dynamical cores, Q. J. Roy. Meteor. Soc., 132, 2943–2975, doi:10.1256/qj.06.12, 2006 4823, 4824, 4825, 4826, 4827, 4831

Jablonowski, C., Lauritzen, P., Nair, R. D., and Taylor, M.: Idealized test cases for the dynamical cores of Atmospheric General Circulation Models: A proposal for the NCAR ASP 2008 summer colloquium, 74 pp., availaible at: http://www-personal.umich.edu/~cjablono/NCAR_ASP_2008_idealized_testcases_29May08.pdf, last access: 15 July 2013, 2008. 4823, 4824, 4827

Lauritzen, P. H., Kaas, E., Machenhauer, B., and Lindberg, K.: Mass-Conservative Version of the Semi-Implicit Semi-Lagrangian HIRLAM, Q. J. Roy. Meteor. Soc., 134, 1583–1595, doi10.1002/qj.307, 2008. 4811

Lauritzen, P. H., Nair, R. D., and Ulrich, P. A.: A conservative semi-Lagrangian multi-tracer transport scheme (CSLAM) on the cubed-sphere grid, J. Comput. Phys., 229, 1401–1429, doi:10.1016/j.jcp.2009.10.036, 2010. 4811

Müller, E. H. and Scheichl, R.: Massively parallel solvers for elliptic PDEs in numerical weather- and climate prediction, 24 pp., available at: http://arxiv.org/abs/1307.2036v1, 2013. 4826

Title Page

Abstract | Introduction

Conclusions | References

Tables | Figures

|◄ | ►|

◄ | ►

Back | Close

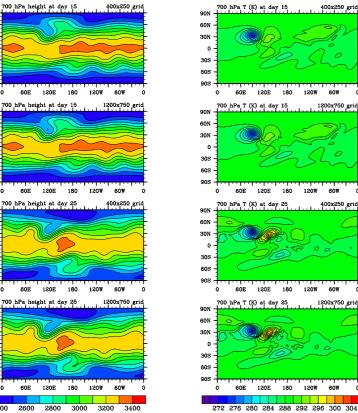Full Screen / Esc

Printer-friendly Version

Interactive Discussion

Nair, R. D., Scroggs, J. S., and Semazzi, F. H. M.: Efficient Conservative Global Transport Schemes for Climate and Atmospheric Chemistry Models, Mon. Weather Rev., 130, 2059–2073, doi:10.1175/1520-0493(2002)130<2059:ECGTSF>2.0.CO;2, 2002. 4820, 4827

Priestley, A.: A quasi-conservative version of the semi-Lagrangian advection scheme, Mon. Weather Rev., 121, 621–629, doi:10.1175/1520-0493(1993)121<0621:AQCVOT>2.0.CO;2, 1993. 4811

Ritchie, H. and Tanguay, M.: A comparison of spatially averaged Eulerian and semi-Lagrangian treatments of mountains, Mon. Weather Rev., 124, 167–181, doi:10.1175/1520-0493(1996)124<0167:ACOSAE>2.0.CO;2, 1996. 4813, 4823

Rochas, M.: ARPEGE Documentation, Part 2, Chapter 6, Météo-France, Toulouse, France, 1990. 4813, 4818

Temperton, C., Hortal, M., and Simmons, A.: A two-time-level semi-Lagrangian spectral global model, Q. J. Roy. Meteor. Soc., 127, 111–129, doi:10.1002/qj.49712757107, 2001. 4815

Tolstykh, M. A.: Vorticity-Divergence Semi-Lagrangian Shallow-Water Model of the Sphere Based on Compact Finite Differences, J. Comput. Phys, 179, 180–200, doi:10.1006/jcph.2002.7050, 2002. 4818

Tolstykh, M. A. and Shashkin, V. V.: Vorticity-divergence mass-conserving semi-Lagrangian shallow-water model using the reduced grid on the sphere, J. Comput. Phys., 231, 4205–4233, doi:10.1016/j.jcp.2012.02.016, 2012. 4819, 4820, 4827

Williamson, D. L., Drake, J. B., Hack, J. J., Jakob, R., and Swartztrauber, P. N.: A standard test set for numerical approximations to the shallow water equations in spherical geometry, J. Comput. Phys., 102, 211–224, 1992. 4823

White III, J. B. and Dongarra, J. J.: High-performance high-resolution tracer transport on a sphere, J. Comput. Phys., 230, 6778–6799, doi:10.1016/j.jcp.2011.05.008, 2011. 4826

Wong, M., Skamarock, W. C., Lauritzen, P. H., and Stull, R. B.: A cell-integrated semi-Lagrangian semi-implicit shallow-water model (CSLAM-SW) with conservative and consistent transport, Mon. Weather Rev., 141, 2545–2560, doi:10.1175/MWR-D-12-00275.1, 2013 4811, 4812, 4827
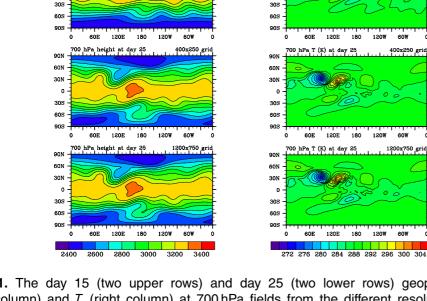
Zerroukat, M. and Allen, T.: A three-dimensional monotone and conservative semi-Lagrangian scheme (SLICE-3D) for transport problems, Q. J. Roy. Meteor. Soc., 138, 1640–1651, doi:10.1002/qj.1902, 2012. 4811

Title Page

Abstract | Introduction

Conclusions | References

Tables | Figures

◄◄ | ►►

◄ | ►

Back | Close

Full Screen / Esc

Printer-friendly Version

Interactive Discussion

Full Screen / Esc

Printer-friendly Version

Interactive Discussion

Fig. 1. The day 15 (two upper rows) and day 25 (two lower rows) geopotential height (left column) and T (right column) at 700 hPa fields from the different resolution SLAV-MC solutions to the mountain induced Rossby wave test case.
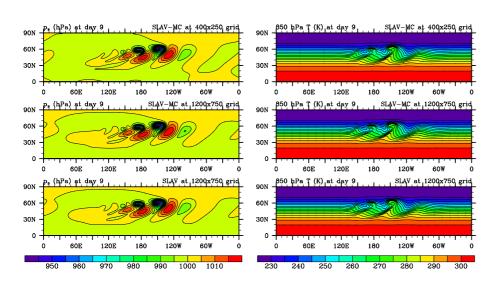
Fig. 2. The day 9 p_s (left column) and T (right column) in Jablonowski and Williamson (2006) test case simulated by the SLAV-MC dynamical core (two upper rows) and standard SLAV dynamical core (lower row).
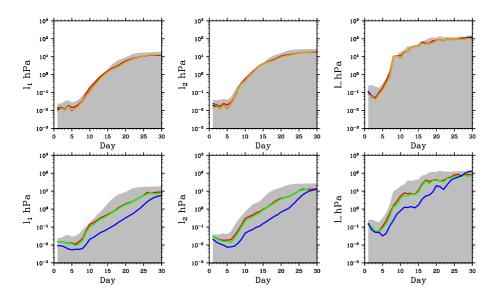
Fig. 3. Time evolution of the l_1, l_2 and l_∞ p_s difference norms. Upper row: difference between the spectral T340 SL reference solution and SLAV-MC solutions on 400×250 (red line), 640×400 (green line), 800×500 (blue line), 1200×750 (orange line) regular lat–lon grids. Lower row: difference between the 1200×750 SLAV-MC solution and the lower resolution SLAV-MC solutions (the line colors are the same as on the upper row). Gray shading presents the uncertainty of reference solutions.

Title Page

Abstract | Introduction

Conclusions | References

Tables | Figures

|◄ | ►|

◄ | ►

Back | Close

Full Screen / Esc

Printer-friendly Version

Interactive Discussion